GEOPHYSICS, VOL. 83, NO. 2 (MARCH-APRIL 2018); P. MR81–MR91, 9 FIGS., 1 TABLE.
10.1190/GEO2017-0293.1

DOI:10.1190/geo2017-0293.1

Seismic-scale dependence of the effective bulk modulus of pore fluid upon water saturation

Uri Wollner[1] and Jack Dvorkin[1]

ABSTRACT

We apply a rock-physics model established from fine-scale data (well or laboratory) to the seismically derived elastic variables (the impedances and bulk density) to arrive at the seismic-scale total porosity, clay content, and water saturation. These three outputs are defined as the volume-averaged porosity, clay content, and porosity-weighted water saturation, respectively. To use the rock-physics model, we need to know how to relate the bulk modulus of the pore fluid to water saturation in the presence of hydrocarbons. At the wellbore-measurement scale, this relation is typically the saturation-weighted harmonic average of the bulk moduli of the water and hydrocarbon. The question posed here is what this relation is at the seismic scale. The method of solution is based on the wellbore-scale data. Specifically, we seek the seismic-scale bulk modulus of the pore fluid that, if used in the rock-physics model, will yield the Backus-upscaled elastic constants at the well from the above-defined seismic-scale petrophysical variables. The answer depends on the vertical distribution of all these variables. By using examples of synthetic and real wells and assuming the lack of hydraulic communication between adjacent rock bodies, we find that this relation trends toward the arithmetic average of the individual bulk moduli of the pore-fluid phases. In fact, it falls in between the arithmetic average and the linear combination of 0.75 arithmetic and 0.25 harmonic averages. We also develop an approximate analytical solution under the assumption of weak elastic and porosity contrasts and for medium-to-high porosity sediment that indicates that the seismic-scale bulk modulus of the pore fluid is close to the arithmetic average of those in the individual layers.

INTRODUCTION

One of the ultimate goals of seismic interpretation is the quantification of the petrophysical properties (lithology and porosity) and conditions (saturation and pore pressure) at the seismic scale. Such interpretation methods can be divided into three categories: deterministic, probabilistic, and stochastic.

The former category uses deterministic "velocity-porosity" transforms or models that are directly applied to either a velocity model of the subsurface or to the impedances and density volumes obtained by way of simultaneous impedance inversion (e.g., Russell, 1988), Bayesian linearized AVO inversion (e.g., Buland and Omre, 2003), or other model-based inversion methods such as stochastic optimization (e.g., Doyen, 2007; Sen and Stoffa, 2013). Examples of deterministic interpretation for petrophysical properties from elastic attributes are given in Angeleri and Carpi (1982), Marion and Jizba (1997), Dolberg et al. (2000), Sams and Saussus (2010), and Arévalo-López and Dvorkin (2016, 2017).

One can also identify different clusters of "elastic lithofacies," such as shale, shaly sand, wet sand, and oil sand, in seismic volumes as part of a probabilistic interpretation approach (e.g., Mukerji et al., 2001; Avseth et al., 2005). Such a classification method is based on previously identified clusters in the elastic domain observed in, for example, well data that represent a training data set. Once these elastic clusters are identified in seismic volumes, they can be interpreted for the respective lithofacies. Rigorous rock-physics models or transforms can be incorporated into this method by expanding the training data set into porosity, fluid, and lithology domains not represented in the original data set.

Stochastic petrophysical interpretation uses information about rock properties collected from a data set and relevant prior information (such as geologic information) to generate an ensemble of possible subsurface models (either of rock properties or facies). Next, a site-specific rock-physics model or transform is used to convert the rock properties to elastic properties in the volume under examina-

Manuscript received by the Editor 8 May 2017; revised manuscript received 25 August 2017; published ahead of production 08 December 2017; published online 29 January 2018.
[1]Stanford University, Stanford, California, USA. E-mail: uriwolln@stanford.edu; dvorkin@stanford.edu.

DOI:10.1190/geo2017-0293.1

tion. These are used to generate synthetic seismograms by convolutional or full-waveform simulation methods emulating the actual survey geometry. Finally, an optimization procedure is carried out to find the set of earth models with the closest match between the synthetic and real seismograms. The output of the stochastic interpretation is a probability density function of rock properties at each depth station. A more general approach to the above-mentioned stochastic interpretation is Bayesian analysis. Examples of such methods can be found in Bortoli et al. (1992), Haas and Dubrule (1994), Eidsvik et al. (2004), Bachrach (2006), Sengupta and Bachrach (2007), Spikes et al. (2007), Grana and Della Rossa (2010), and Grana (2016).

The required rock-physics transform that is inherent to all these methods can be either derived as a best-fit regression from available laboratory (e.g., Han, 1986) or well-log data, or it can be based on theoretical rock-physics models calibrated at the well. The latter process is called rock-physics diagnostics (Dvorkin et al., 2014). In some cases, the transform can be simply assumed during frontier exploration based on geologic and depositional information.

In this work, we concentrate on the interpretation of the seismic-scale elastic variables for the petrophysical variables rather than the procedure of the impedance inversion of seismic data. By seismic scale, we mean the size of an individual reading in a volume of seismically derived impedances. This size can be on the order of tens of feet as opposed to the wellbore scale, where this size is approximately 0.3 m (1 ft).

To formulate the inverse problem of estimating petrophysical variables from seismically inverted impedances as well as bulk density, we first relate the impedances to the bulk (K) and shear (G) moduli under the assumption of isotropy as

$$I_p = \sqrt{\rho_b(K + 4G/3)}; \quad I_s = \sqrt{\rho_b G}. \tag{1}$$

A rock-physics model usually relates these elastic moduli to the total porosity ϕ, the elastic moduli of the isotropic mineral matrix, K_s and G_s, as well as to the bulk modulus of the pore fluid K_f,

$$K = F_K(\phi, K_s, G_s, K_f); \quad G = F_G(\phi, K_s, G_s), \tag{2}$$

where F_K and F_G are the rock-physics transforms.

Notice that only K depends on K_f because, according to Gassmann's (1951) assumption, G is not affected by the pore fluid.

The bulk density ρ_b depends on the total porosity ϕ and the density of the mineral matrix ρ_s and that of the pore fluid ρ_f as

$$\rho_b = (1 - \phi)\rho_s + \phi\rho_f, \tag{3}$$

where, in a simple case of binary quartz/clay mineralogy,

$$\rho_s = (1 - C)\rho_Q + C\rho_C, \tag{4}$$

where ρ_Q and ρ_C are the densities of quartz and clay, respectively.

The density of the pore fluid ρ_f is a function of those of water ρ_w and gas ρ_g and the water saturation S_w

$$\rho_f = S_w\rho_w + (1 - S_w)\rho_g. \tag{5}$$

Notice now that K in equation 2 is a direct function of K_f rather than S_w. Hence, to resolve equations 1–5 for ϕ, C, and S_w, we need to know how to relate K_f to S_w. This is the ultimate question we pose here.

The solution is not obvious because, as previous works (e.g., Domenico, 1976; Cadoret, 1993; Brie et al., 1995; Wollner and Dvorkin, 2016; Dvorkin and Wollner, 2017) show, K_f is not necessarily the harmonic average of the bulk moduli of the water and hydrocarbon as commonly assumed where the fluid phases coexist at the pore scale. This observed deviation from the harmonic average is related to the absence of hydraulic communication between domains in rock saturated with different fluids, often called patchy saturation, which is especially prevalent at the seismic scale.

In addition, this deterministic approach raises an important basic-science issue. A transform or model (e.g., granular or inclusion models) established at one scale of measurement (0.15 m [approximately 0.5 ft] in the well) may not necessarily be valid at a different scale (30.4 m [approximately 100 ft] in seismic data). Although the issue may not directly affect the interpretation results under the stochastic/Bayesian framework, it does so in the deterministic approach.

Dvorkin and Wollner (2017) show through forward modeling that a rock-physics model established from fine-scale (e.g., borehole-scale) measurements can accurately predict the elastic properties of heterogeneous media at a coarser scale (e.g., seismic-scale) given the appropriate inputs are used. Specifically, they consider the case of layered geometry, where the adjacent layers do not hydraulically communicate at the time scale of elastic-wave propagation. Then, the inputs to the model should be the arithmetically volume-averaged porosity and clay content (in a simple quartz/clay setting) and, approximately, the arithmetically volume-averaged bulk modulus of the pore fluid. In other words, at the seismic scale, the mixing law that relates water saturation to the effective pore-fluid bulk modulus in a layered medium should not be computed using the harmonic average of individual pore-fluid bulk moduli weighted by their volume fraction (as is usually assumed at the well scale). Hence, deterministic interpretation of rock properties from seismic-scale elastic attributes can lead to large errors in the estimates if the appropriate mixing law is not considered.

This work addresses the issue of such mixing laws within the deterministic interpretation approach. The issue of impedance inversion is beyond the scope of this paper. We assume that Backus (1962) averaging applied to fine-scale elastic properties is representative of the coarse-scale elastic parameters (see Appendix A). Because rock-physics models or transforms calibrated to well data are site specific, it is reasonable to assume that the mixing laws relating water saturation to the seismic-scale pore-fluid bulk modulus are site specific as well. Here, we propose a methodology to obtain locally calibrated mixing laws and use forward modeling to understand how reservoir thickness and water saturation affect these laws. Finally, we implement this method on real well data from a clastic environment and deterministically interpret the upscaled P- and S-wave impedances and density for the seismic-scale total porosity, clay content, and water-saturation profiles.

METHODS

We propose to relate K_f to S_w by using well data. In real wells, the data should be sufficient to compute the total porosity and water saturation, as well as to quantify the mineralogy. We also require the bulk density and the P- and S-wave velocity (V_P and V_S,

respectively), as well as the densities and bulk moduli of the components of the pore fluid.

Once such a data set is available, the question becomes how to relate K_f to S_w at a coarser (seismic) scale. To approach this problem, we

1) Apply the running window Backus (1962) average to the isotropic elastic moduli at the well to compute the upscaled elastic stiffnesses $\bar{C}_{33}$ and $\bar{C}_{44}$ (see Appendix A). These variables are the upscaled P-wave $\bar{H} = \bar{C}_{33}$ and S-wave moduli $\bar{G} = \bar{C}_{44}$ in the vertical direction. We define the respective bulk modulus $\bar{K}$ as

$$\bar{K} = \bar{H} - \frac{4}{3}\bar{G}. \tag{6}$$

Although Backus (1962) averaging produces an anisotropic (vertical transverse isotropic) effective medium, we assume for simplicity that, with regard to fluid substitution, we can treat the layered sequence as an isotropic material with these bulk, shear, and compressional moduli. This approximation is justified in the presence of weak elastic contrast (Mavko and Bandyopadhyay, 2009). Specifically, the Thompsen's parameter δ has to be small. In all our examples, it does not fall outside the -0.05 to 0.05 interval. Mavko and Bandyopadhyay (2009) show that in this case, the difference between the isotropic and anisotropic Gassmann's (1951) fluid substitution for the P-wave velocity is less than 1.5%.

The upscaled bulk density $\bar{\rho}_b$ is obtained from the well-scale ρ_b by arithmetically averaging the latter using the same running window as in the Backus averaging. The upscaled impedances $\bar{I}_p$ and $\bar{I}_s$ in the vertical direction are computed as

$$\bar{I}_p = \sqrt{\bar{\rho}_b(\bar{K} + 4\bar{G}/3)}; \quad \bar{I}_s = \sqrt{\bar{\rho}_b \bar{G}}, \tag{7}$$

and the upscaled Poisson's ratio (PR) $\bar{\nu}$ as

$$\bar{\nu} = \frac{1}{2}\frac{\bar{I}_p^2/\bar{I}_s^2 - 2}{\bar{I}_p^2/\bar{I}_s^2 - 1}. \tag{8}$$

Note that we use the Backus-upscaled elastic properties as proxies to those obtained from seismic data by impedance inversion. We discuss this approximation in Appendix A and show that if the running window size is smaller than or equal to approximately one-sixteenth of the wavelength, the synthetic seismograms from the wellbore-scale elastic curves and from those obtained by Backus averaging are practically identical.

2) By using the same running window as for the Backus average, we compute the arithmetically upscaled total porosity $\bar{\phi}$ and the clay content $\bar{C}$. Instead of arithmetically upscaling the S_w curve, we wish to upscale the fractional volume of the hydrocarbon in the interval. At each depth station, this volume is $\phi(1 - S_w)$. Hence, the fractional volume of the hydrocarbon within the averaging window, assuming that the thickness of each layer is the same, is

$$f_{\mathrm{HC}} = \sum_{i=1}^{N} \phi_i(1 - S_{w,i}) \Big/ \sum_{i=1}^{N} \phi_i, \tag{9}$$

where N is the number of the layers in the running window and the subscript "i" refers to the properties of ith layer. As a result, the upscaled water saturation $\bar{S}_w$ is computed as

$$\bar{S}_w = \sum_{i=1}^{N} \phi_i S_{w,i} \Big/ \sum_{i=1}^{N} \phi_i. \tag{10}$$

This is the definition of averaged water saturation that we aspire to obtain from the seismically derived impedances and bulk density.

3) The dry-rock bulk modulus K_{Dry} is computed at each depth station in the interval using isotropic Gassmann's (1951) fluid substitution. To conduct this operation, we obtain the effective bulk modulus of the pore fluid K_f as

$$\frac{1}{K_f} = \frac{S_w}{K_w} + \frac{1 - S_w}{K_g}, \tag{11}$$

which is the S_w-weighted harmonic average of the bulk moduli of water K_w and gas K_g. The bulk modulus of the mineral matrix required for this operation is computed at each depth station using the clay content C, for the case of a simple quartz/clay mineralogy, with Hill's (1952) average. The upscaled dry-rock P-wave modulus ($\bar{H}_{\mathrm{Dry}}$) is computed using the same Backus averaging window applied to the well-scale H_{Dry} defined as $H_{\mathrm{Dry}} = K_{\mathrm{Dry}} + 4G/3$. The upscaled dry-rock modulus $\bar{K}_{\mathrm{Dry}}$ is then computed using $\bar{H}_{\mathrm{Dry}}$ and $\bar{G}_{\mathrm{Dry}} = \overline{G}$ in equation 6.

4) Finally, we use the isotropic Gassmann's (1951) fluid-substitution equation to find the as yet unknown upscaled bulk modulus of the pore fluid $\bar{K}_f$ as

$$\bar{K}_f = \bar{K}_s \frac{\bar{\phi}\left(\frac{\bar{K}}{K_s - \bar{K}} - \frac{\bar{K}_{\mathrm{Dry}}}{K_s - \bar{K}_{\mathrm{Dry}}}\right)}{1 + \bar{\phi}\left(\frac{\bar{K}}{K_s - \bar{K}} - \frac{\bar{K}_{\mathrm{Dry}}}{K_s - \bar{K}_{\mathrm{Dry}}}\right)}, \tag{12}$$

where $\bar{K}_s$ is the upscaled bulk modulus of the mineral phase computed from the upscaled clay content $\bar{C}$ by using Hill's (1952) average.

The $\bar{K}_f$ and $\bar{S}_w$, thus upscaled along the interval using the selected running averaging window, are related to each other to find the required dependence between these two variables.

What follows is a numerical investigation of the K_f to S_w relation at a coarser scale with vertical synthetic wells built on the basis of a selected rock-physics model that relates the elastic properties to porosity, mineralogy, and water saturation. We also assume that at each depth station where water and hydrocarbons (gas) are present, the effective bulk modulus of the pore fluid K_f required by the model is related to S_w in equation 11.

RESULTS

Synthetic-well examples

Figure 1 shows three synthetic wells, where a gas reservoir is placed in between two identical shale layers. The only difference between the wells is the thickness of the gas sand. When computing the elastic properties, we used the total porosity and clay content shown in Figure 1 (binary quartz/clay mineralogy) as inputs to the constant-cement model (Dvorkin et al., 2014), in which the differential pressure was 16.5 MPa, the coordination number was 14, the critical porosity was 0.40, and shear correction factor was 1. The densities and elastic moduli of the rock constituents used in our modeling are listed in Table 1. In this example, we used the "standard" clay properties from Table 1.

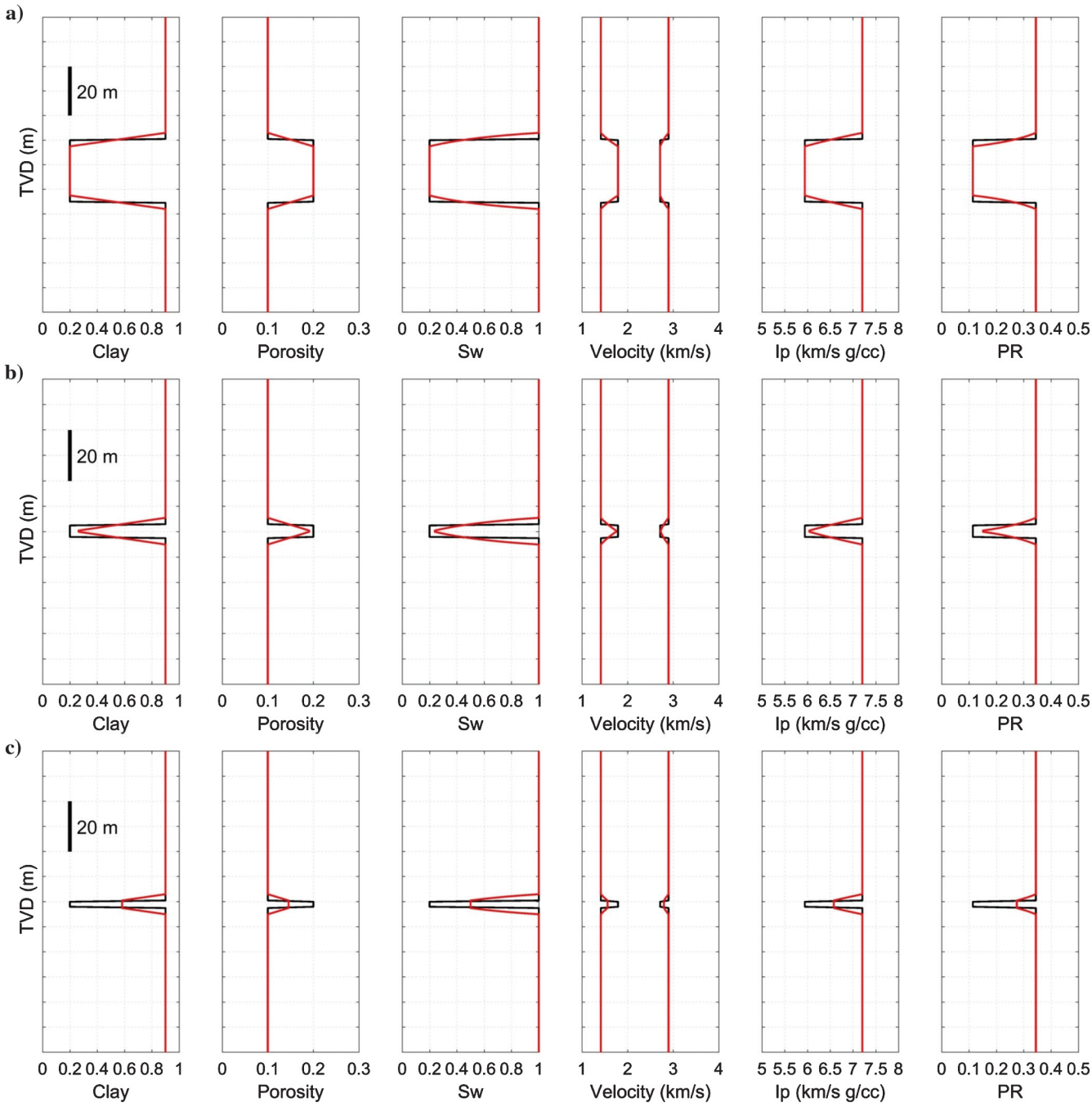

Figure 1. Three synthetic wells, where a gas reservoir is placed in between two shale layers. In each row, the tracks (left to right) show the clay content, the total porosity, water saturation, P- and S-wave velocity, P-wave impedance, and PR versus the true vertical depth (TVD). The well-scale curves are black, whereas the upscaled curves (5 m running window) are red. The three wells shown are identical except for the thickness of the reservoir that is (a) 25, (b) 5, and (c) 2.5 m.

DOI:10.1190/geo2017-0293.1

All property profiles shown in Figure 1 were upscaled as explained in the previous section using a 5 m running window (approximately one-sixteenth of the wavelength). The respective upscaled profiles are plotted in red. Next, these upscaled profiles were used to compute the upscaled bulk modulus of the pore fluid $\bar{K}_f$ at each depth station according to equation 12. It is plotted versus the upscaled $\bar{S}_w$ in Figure 2.

Also in Figure 2, we plot, versus $\bar{S}_w$, the bulk modulus of the pore fluid upscaled from the well-scale K_f and, using the same running window, with the arithmetic (AR) and harmonic (HR) averages, as well as a linear combination of these two averages 0.75 AR + 0.25 HR, as originally proposed by Dvorkin and Wollner (2017).

In all three synthetic wells, the relation between $\bar{K}_f$ and $\bar{S}_w$ is the same. However, we only observe parts of the $\bar{K}_f$ versus $\bar{S}_w$ trend where the reservoir is relatively thin (Figure 2b and 2c) and $\bar{S}_w$ does not span the entire range between 0.20 and 1.00, as opposed to the thick reservoir case (Figure 2a). In the lower $\bar{S}_w$ range, $\bar{K}_f$ appears to be very close to the 0.75 AR + 0.25 HR linear combination. At a higher saturation, it falls in between AR and 0.75 AR + 0.25 HR. The harmonic average HR falls far below $\bar{K}_f$.

In the next example (Figure 3), we use the same setup as shown in Figure 1, but the thickness of the reservoir is a constant 25 m, whereas S_w in the reservoir varies from (a) 0.20 to (b) 0.50 and to (c) 0.75 between the wells. The upscaling was conducted in the same way as in the first example. The resulting $\bar{K}_f$ is plotted versus $\bar{S}_w$ in Figure 4 in the same way as it is done in Figure 2 for the first example.

The results shown in Figure 4a are identical to those shown in Figure 2a. In the remaining two cases (b and c), because the reservoir is thick and, hence, the entire saturation range is still present in the $\bar{S}_w$ profiles, the $\bar{K}_f$ versus $\bar{S}_w$ relations span the entire ranges between water saturation in the reservoir and 100%. Once again, the 0.75 AR + 0.25 HR approximation is close to $\bar{K}_f$ in the lower parts of the $\bar{S}_w$ ranges in each case.

Table 1. Densities and elastic moduli of the materials used in modeling examples.

Material	Density (g/cm^3)	Bulk modulus (GPa)	Shear modulus (GPa)
Quartz	2.65	36.60	45.00
Clay (standard)	2.65	21.00	7.00
Clay (soft)	2.65	10.50	3.50
Feldspar	2.65	75.60	25.60
Water	1.01	2.61	0.00
Gas	0.18	0.06	0.00

Real-well example

In this section, we explore the $\bar{K}_f$ versus $\bar{S}_w$ relations using three wells (X, Y, and Z) drilled through a gas reservoir. This data set was examined by Wollner et al. (2017), where a rock-physics model (the constant-cement model) was found to accurately match the P-wave data. The input parameters were the differential pressure 16.5 MPa, coordination number 14, critical porosity 0.40, and shear correction factor 1. The S-wave data appeared to be spurious and were corrected according to this model. The mineralogy in this sediment was ternary, quartz, clay, and feldspar, with assumed constant feldspar content of 20% in the nonclay part of the mineral matrix. It was also established that the appropriate elastic moduli for the clay were 10.5 GPa for the bulk and 3.5 GPa for the shear moduli. These are the properties of "soft clay" listed in Table 1. The rock properties for these wells are plotted versus the true vertical depth (TVD) in Figure 5.

The same methodology as used with the synthetic wells was applied to these data to obtain the $\bar{K}_f$ versus $\bar{S}_w$ relation. The results are shown in Figure 6a–6c for wells X, Y, and Z, respectively. The $\bar{K}_f$ versus $\bar{S}_w$ trends are slightly different from each other between the wells and also bifurcate in X and Z due to multiple reservoir layers present in these wells.

To obtain a single general trend applicable to the entire volume containing the three wells, we binned the $\bar{S}_w$ axes in Figure 6a–6c into 15 equal intervals between the minimum $\bar{S}_w$ and $\bar{S}_w = 1$ and then computed the means of $\bar{K}_f$ values in each bin for all three wells together. The result is displayed in Figure 6d.

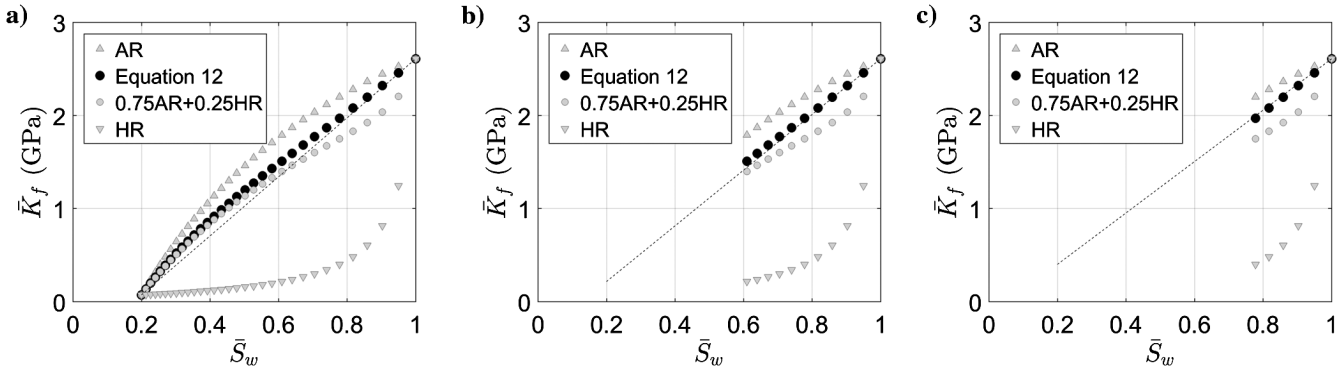

Figure 2. Upscaled K_f (equation 12) versus upscaled S_w (equation 10) for the three pseudowells (a-c) shown in Figure 1 (black circles). The AR running average is shown as gray pointed upward triangles; 0.75 AR + 0.25 HR is shown as gray circles; and HR is shown as gray pointed-downward triangles. The dashed line is a linear connector between the 0.20 and 1.00 saturation end points.

It appears that in this example, the AR approximation is practically the same as the binned and averaged $\bar{K}_f$ values in the entire $\bar{S}_w$ interval.

Finally, to implement this result, we interpret the Backus-upscaled (5 m running window) $\bar{I}_p$ and $\bar{I}_s$ as well as the arithmetically upscaled $\bar{\rho}_b$ for the seismic-scale porosity ($\bar{\phi}_{\text{Interp}}$), clay content ($\bar{C}_{\text{Interp}}$), and water saturation ($\bar{S}_{w\text{Interp}}$) in each of the three wells. This interpretation is based on the constant-cement model established for these wells (Wollner et al., 2017), which provides the rock-physics transform functions F_K and F_G in equation 2. To solve this inverse problem, we supplement equations 1–5 with the $\bar{K}_f$ versus $\bar{S}_w$ relation shown in Figure 6d as black circles.

The resulting $\bar{\phi}_{\text{Interp}}$, $\bar{C}_{\text{Interp}}$, and $\bar{S}_{w\text{Interp}}$ are shown in Figure 7 in black. These values are very close to the $\bar{\phi}$, $\bar{C}$, and $\bar{S}_w$ (bold gray in Figure 7) upscaled from ϕ, C, and S_w at the wells with a 5 m running window.

The same interpretation is next conducted using the 0.75 AR + 0.25 HR approximation shown in red in Figure 6d. The results are

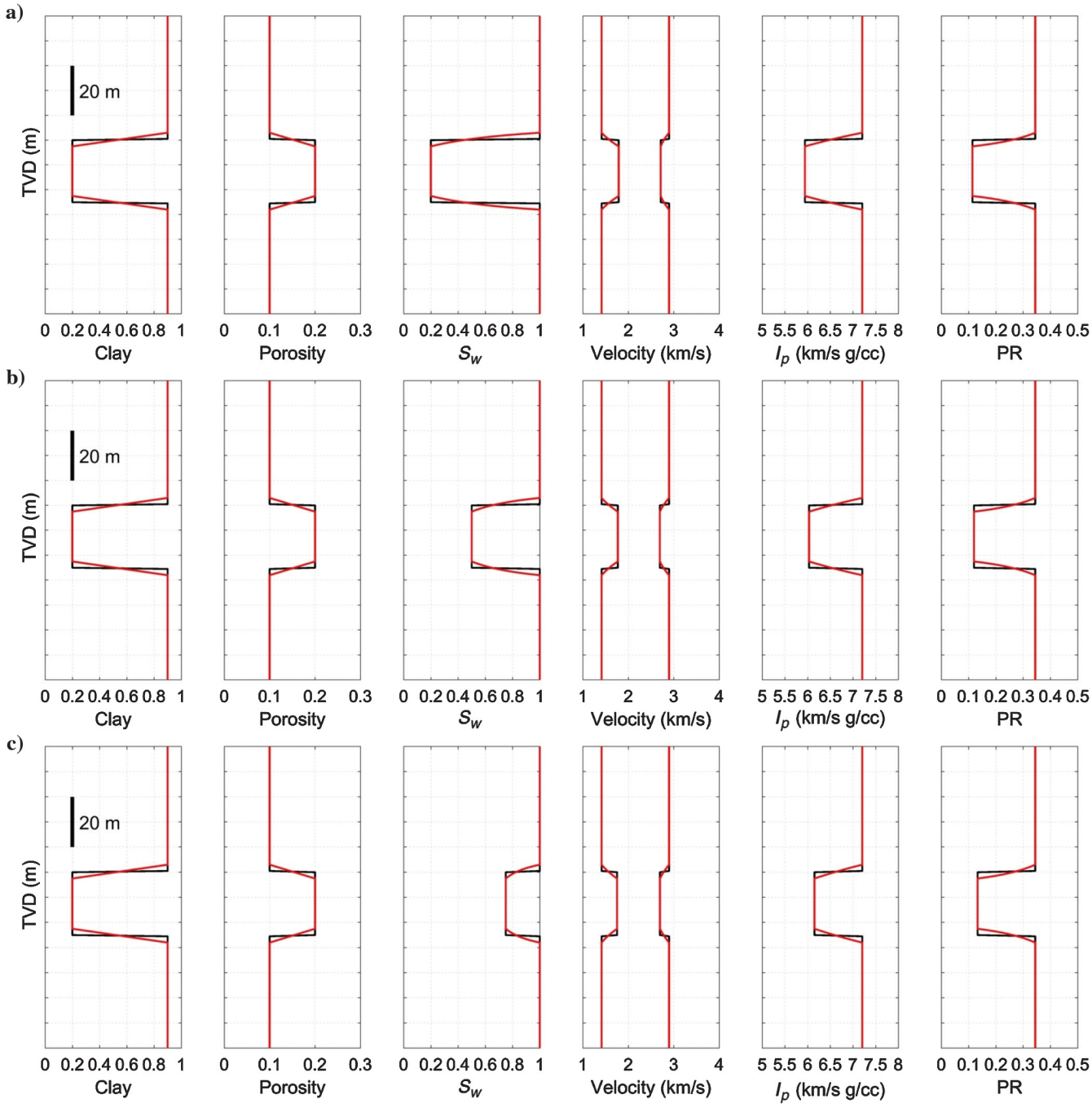

Figure 3. The same as Figure 1, but with a constant reservoir thickness (25 m) and varying water saturation.

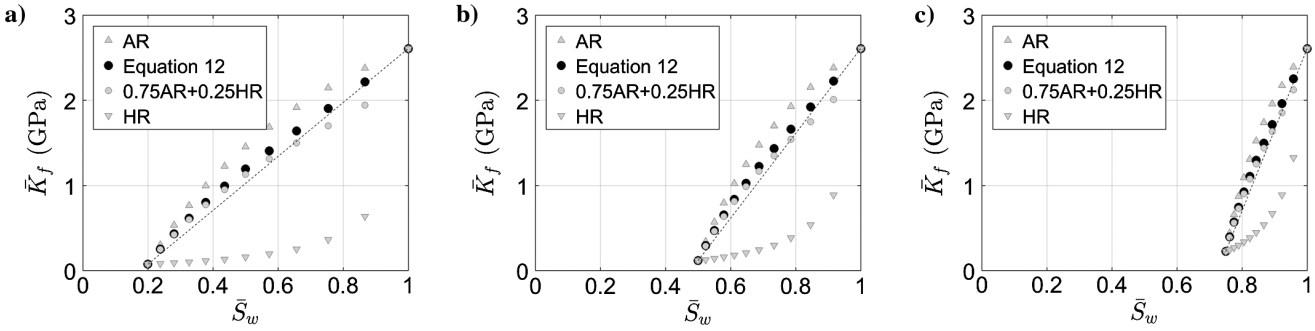

Figure 4. The same as Figure 2, but for the cases shown in Figure 3.

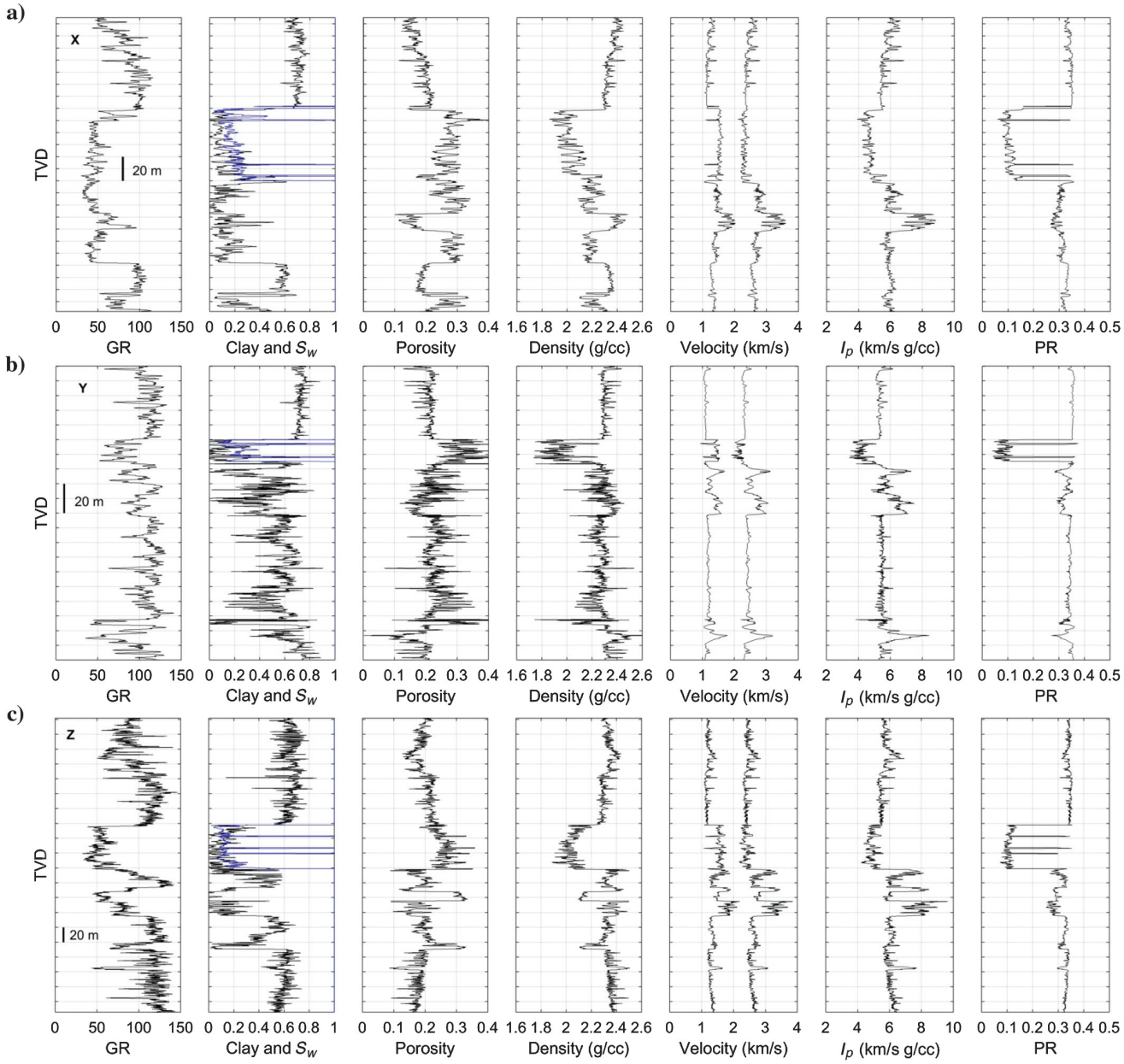

Figure 5. Depth profiles of gamma ray; clay content in black and S_w in blue; the total porosity; bulk density; V_P and V_S; I_p; and PR for wells (a) X, (b) Y, and (c) Z.

shown in red in Figure 7. They are very close to the results of the first interpretation (black curves in Figure 7).

DISCUSSION

Essentially, all effective medium models used in rock physics treat a heterogeneous volume of rock as spatially homogeneous, meaning that they relate a single set of elastic constants to a single set of petrophysical properties and conditions, such as porosity, clay content, stress, and water saturation. In other words, rock physics treats a volume of rock as a point in space. The porosity, mineralogical fractions, and water saturation of an effective medium is the volume average of these quantities. However, the effective elastic constants of the medium depend on the spatial configuration of the elastic bodies composing the rock volume. For the case of layered geometry, as is assumed here, Dvorkin and Wollner (2017) show that an isotropic rock-physics transform linking the elastic to petrophysical rock properties can approximately describe such a volume treated as an effective medium. Yet, in their work, one link was missing: how to relate the "effective" bulk modulus of the pore fluid containing more than one constituent to the average water saturation. This is the subject of our present investigation.

This relation is required in forward modeling because many rock-physics models compute first the dry-frame elastic constants and then obtain the saturated-rock constants via fluid substitution. In contrast, these models can also be used in the inverse mode to derive the petrophysical properties from elastic measurements at the seismic scale. Once again, an appropriate $\bar{K}_f$-$\bar{S}_w$ relation is required for this purpose.

Here, we show examples of such interpretation using $\bar{K}_f$-$\bar{S}_w$ relations established via forward modeling at synthetic and real wells. These relations are much closer to the arithmetic than to the harmonic average of the individual bulk moduli of the fluid components. The synthetic examples presented in Figures 1 and 2 suggest that regardless of whether the reservoir is resolved at a coarse scale or not, the $\bar{K}_f$-$\bar{S}_w$ relations remain the same given that only the thickness of the reservoir changes. On the other hand, Figures 3 and 4 show that if the hydrocarbon content in the reservoir changes, the $\bar{K}_f$-$\bar{S}_w$ relations vary as well. Hence, to minimize the uncertainty in an interpretation of seismic data, $\bar{K}_f$-$\bar{S}_w$ relations should be locally calibrated.

Such a locally calibrated relation based on well data is shown in Figure 6d. It is used to interpret the coarse-scale impedances and bulk density in the wells for the total porosity, clay content, and water saturation (Figure 7). This interpretation is in agreement with these variables independently upscaled in the well, no matter whether we use the averaged relation for the three wells or its 0.75 AR + 0.25 HR approximation. This fact is not trivial because we did not use a local relation at each well, but rather their binned average.

Still, for the same reason, our interpretation may seem overly optimistic. To address this concern, we repeat the interpretation process in each of the three wells, but now based on only the binned and averaged $\bar{K}_f$-$\bar{S}_w$ relations computed in well X. The results are displayed in Figure 8 (black). Once again, the agreement between the interpreted and the true upscaled quantities is quite satisfactory.

In frontier exploration, where well data are unavailable, the required $\bar{K}_f$-$\bar{S}_w$ relations must be somehow approximated. One way is to assume a rock-physics model consistent with local geology and then use this model to construct pseudowells and compute the required $\bar{K}_f$-$\bar{S}_w$ trends as shown above. Of course, to construct such wells and constrain the resulting relations, we need prior information (most likely an assumption) about S_w ranges in the reservoir. A set of such "training" wells can be constructed statistically as in Grana and Della Rossa (2010). Then, we will have a distribution of the $\bar{K}_f$-$\bar{S}_w$ curves allowing for introducing uncertainty into our deterministic framework.

If no such information is available, S_w can be assumed constant. The bulk modulus of the pore fluid at this endpoint in the $\bar{K}_f$-$\bar{S}_w$ plane can be computed as the harmonic average of the individual bulk moduli of the fluid components weighted by this S_w value. This endpoint can then be connected to the $\bar{S}_w = 100\%$ endpoint by either a straight line representing the arithmetic average or by a 0.75 AR + 0.25 HR curve. An example of using this linear combination and assuming the $\bar{S}_w = 0$ endpoint, is shown in Figure 8 in red. As expected, because the S_w endpoint was chosen zero instead of approximately 20%, the interpreted S_w (red in Figure 8) is underestimated. At the same time, the interpreted porosity and clay content match the upscaled measurements very well simply because the sensitivity of the elastic constants to water saturation in the low S_w range is small.

Finally, let us note that the interpretation results may strongly depend on the input parameters. Therefore, if the seismic-scale impedances and bulk density as obtained, for example, from simul-

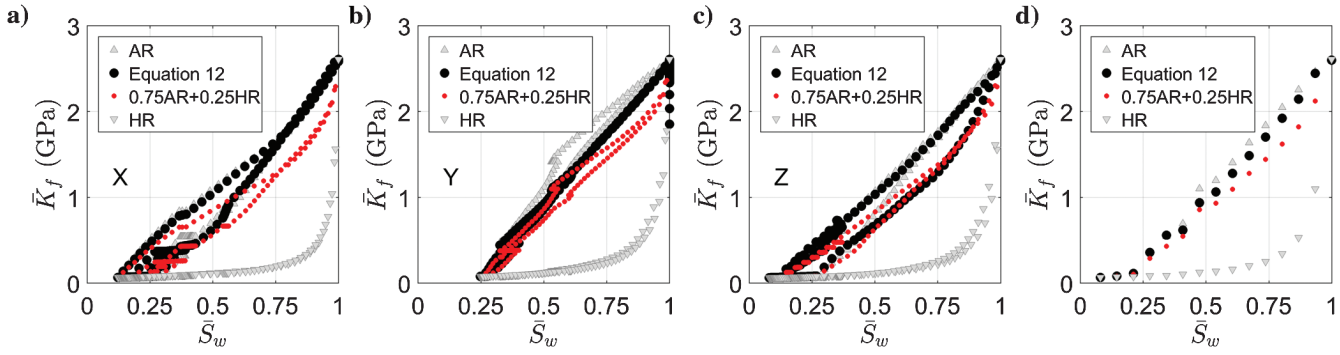

Figure 6. The same as Figures 2 and 4, but for the wells (a) X, (b) Y, and (c) Z shown in Figure 5. For visualization purposes, 0.75 AR + 0.25 HR is shown in red. The binned and averaged results (as explained in the text) are shown in (d).

taneous impedance inversion significantly differ from these properties measured in the well, the resulting interpreted values will likely not match the well data either. To quantify such a deterministic mismatch, statistical uncertainty can be introduced, together with the site-specific $\bar{K}_f$-$\bar{S}_w$ relations, to obtain probability distributions for the seismic-scale $\bar{\phi}$, $\bar{C}$, and $\bar{S}_w$ at each depth level (e.g., Grana and Della Rossa, 2010). Of course, the significance of the mixing law to the interpretation process is reduced if the elastic contrast between the bulk moduli of individual pore-fluid phases is not large (Arévalo-López and Dvorkin, 2017).

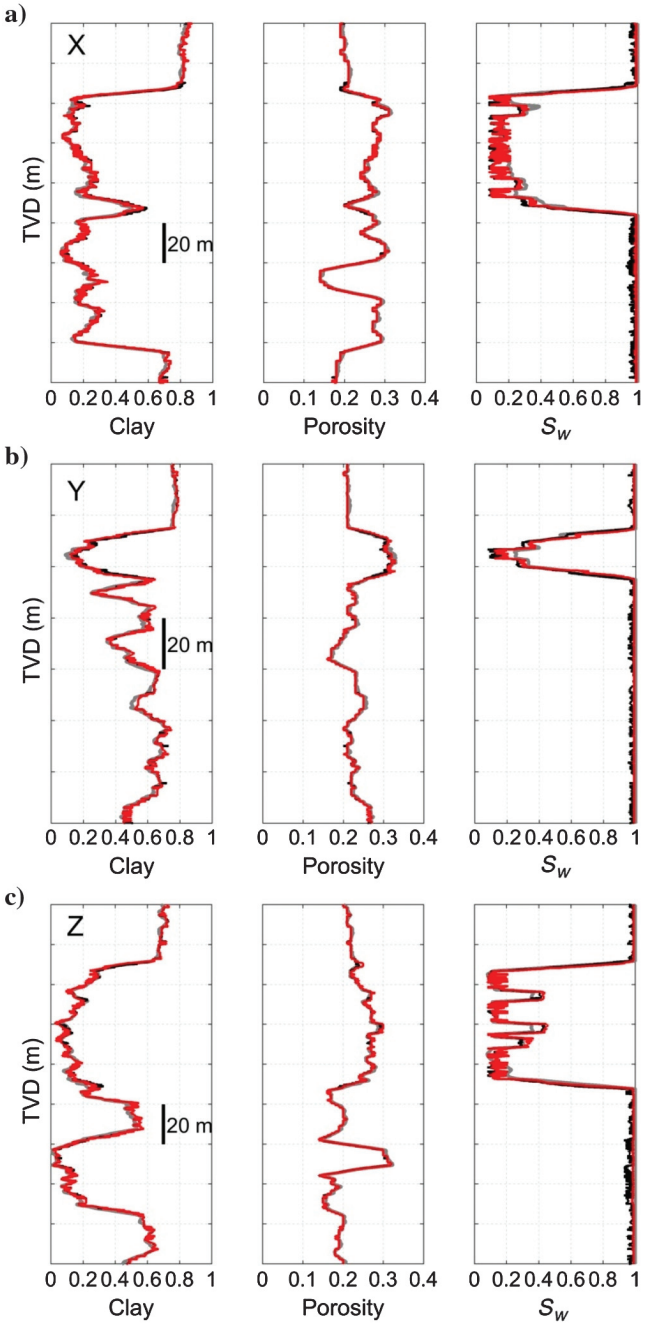

Figure 7. Depth profiles of upscaled and interpreted total porosity, clay content, and water saturation for wells (a) X, (b) Y, and (c) Z obtained as explained in the text. The bold gray curves are the upscaled well data. The black curves are the interpreted variables using the fluid bulk modulus versus water-saturation relation shown in black in Figure 6d. The red curves are the interpreted variables using the 0.75 AR + 0.25 HR approximation (the red symbols in Figure 6d).

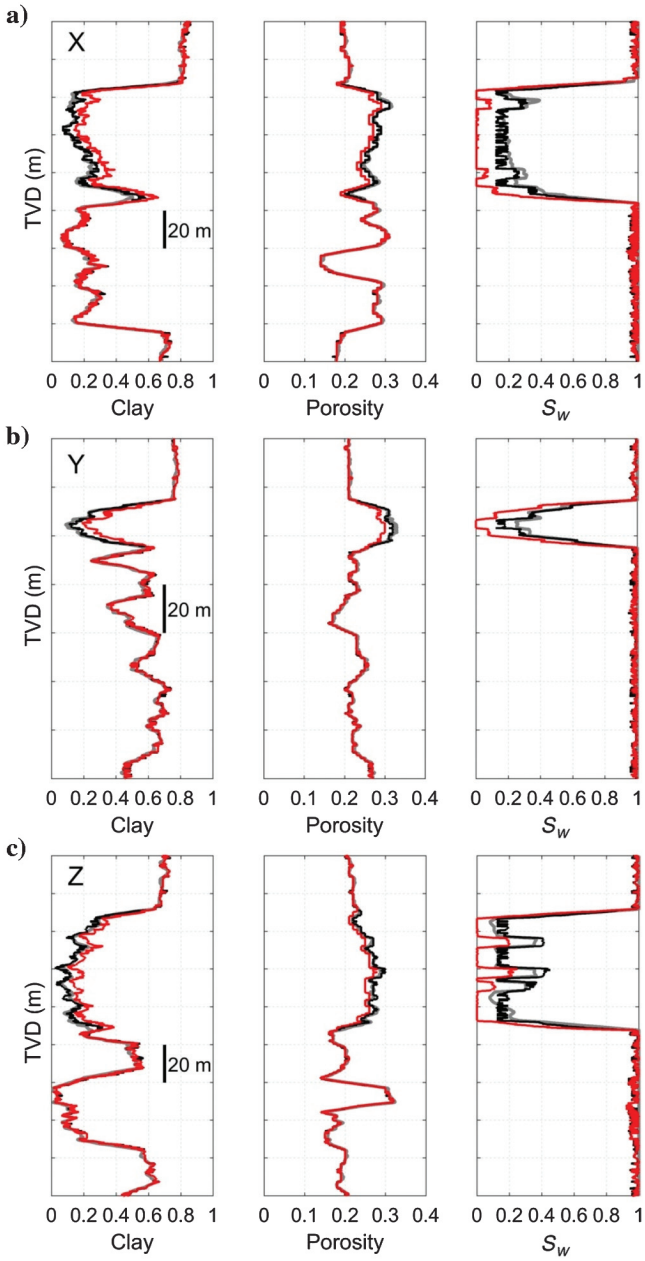

Figure 8. The same as Figure 7, but with the interpreted curves computed based on the binned and averaged bulk modulus-saturation relation computed only in well X. The bold gray curves are the upscaled well data. The black curves are the interpreted variables. The red curves are the interpreted variables using the 0.75 AR + 0.25 HR approximation established assuming zero water saturation in the reservoir.

CONCLUSION

The specific technical objective of this work appears to be very specialized and narrow — relating the effective bulk modulus of the pore fluid to water saturation at the seismic scale. Yet, this task appears to be a crucial element of a much more general and important problem, which is rock-physics-based interpretation of simultaneous impedance inversion results for petrophysical variables, porosity, clay content, and water saturation. The results, now that they have been rigorously derived, also appear almost obvious. Indeed, in the examples provided here, a $\bar{K}_f$-$\bar{S}_w$ relation is much closer to that for the patchy saturation pattern than to the uniform one. Still, we feel that to improve the quality of interpretation, this relation has to be locally calibrated using well data. The methodology presented here is valid for any rock-physics model and, hence, it should be used with a site-specific transform.

ACKNOWLEDGMENTS

This work was supported by the Stanford Rock Physics and Borehole Geophysics project. We thank all the reviewers and, specifically, N. Saxena and D. Grana for meaningful and constructive comments.

APPENDIX A

BACKUS AVERAGE

A linearly elastic isotropic body can be described by the following fourth-order stiffness tensor C_{ij} written in Voigt notation as

$$C_{ij} = \begin{bmatrix} C_{11} & C_{12} & C_{12} & 0 & 0 & 0 \\ C_{12} & C_{11} & C_{12} & 0 & 0 & 0 \\ C_{12} & C_{12} & C_{11} & 0 & 0 & 0 \\ 0 & 0 & 0 & C_{44} & 0 & 0 \\ 0 & 0 & 0 & 0 & C_{44} & 0 \\ 0 & 0 & 0 & 0 & 0 & C_{44} \end{bmatrix}, \quad \text{(A-1)}$$

where $C_{11} = K + 4G/3$, $C_{12} = K - 2G/3$, and $C_{44} = G$. Backus (1962) shows that in the long-wavelength limit, a medium composed of a sequence of isotropic layers with the axis of layering perpendicular to the x_3-direction can be represented as an effective medium having transverse isotropy with the following elastic constants:

$$\begin{aligned} \bar{C}_{11} &= \bar{C}_{22} = \left\langle \frac{4G(\lambda+G)}{\lambda+2G} \right\rangle + \left\langle \frac{1}{\lambda+2G} \right\rangle^{-1} \left\langle \frac{\lambda}{\lambda+2G} \right\rangle^{2}, \\ \bar{C}_{12} &= \bar{C}_{21} = \left\langle \frac{2G\lambda}{\lambda+2G} \right\rangle + \left\langle \frac{1}{\lambda+2G} \right\rangle^{-1} \left\langle \frac{\lambda}{\lambda+2G} \right\rangle^{2}, \\ \bar{C}_{33} &= \left\langle \frac{1}{\lambda+2G} \right\rangle^{-1}, \\ \bar{C}_{13} &= \bar{C}_{23} = \bar{C}_{31} = \bar{C}_{32} = \left\langle \frac{1}{\lambda+2G} \right\rangle^{-1} \left\langle \frac{\lambda}{\lambda+2G} \right\rangle, \\ \bar{C}_{44} &= \bar{C}_{55} = \left\langle \frac{1}{G} \right\rangle^{-1}, \\ \bar{C}_{66} &= \langle G \rangle^{-1}, \end{aligned} \quad \text{(A-2)}$$

where $\lambda = K - 2G/3$ and $\langle \cdot \rangle$ is the arithmetic averaging operator across all layers. For instance, given material quantity $\mathbf{m}$, its average value for a stack of N layers is given by

$$\langle \mathbf{m} \rangle = \sum_{k=1}^{N} f_k m_k; \quad \sum_{k=1}^{N} f_k = 1, \quad \text{(A-3)}$$

with f_k and m_k being the volume fraction and the material quantity of kth layer, respectively.

In this work, we assume that the Backus-upscaled elastic properties in the vertical (x_3) direction can serve as proxies for the seismically derived impedance from simultaneous impedance inversion. To test this assumption, we compare the normal-incidence full-waveform synthetic seismograms obtained from (1) the borehole-scale elastic properties and (2) Backus-upscaled elastic properties. If these two seismograms are identical, our assumption is corroborated.

An example of this numerical experiment using wells X, Y, and Z (see the main text) is shown in Figure A-1. If the size of the upscaling window is 5 m (approximately one-sixteenth of the wavelength) or smaller, the two seismograms are identical in all three wells (Figure A-1a). If the window size is 15 m, the seismograms are qualitatively the same apart from small qualitative mismatch in peaks and troughs (Figure A-1b).

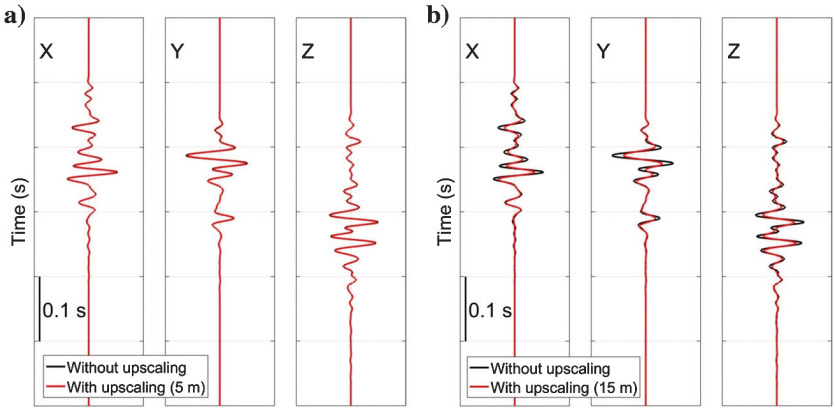

Figure A-1. Synthetic seismograms in wells X, Y, and Z generated using the borehole-scale elastic data (black) and Backus-upscaled elastic data (red). (a) 5 m upscaling window and (b) 15 m upscaling window.

APPENDIX B

ANALYTICAL APPROXIMATION

Here, we present an asymptotic analytical approximation to our solution obtained under the assumption of small elastic contrast between the layers resolved in wellbore data.

Specifically, let us assume that

$$\begin{aligned} &|K_{\mathrm{Dry}}^{(i)} - \langle K_{\mathrm{Dry}} \rangle| / \langle K_{\mathrm{Dry}} \rangle \ll 1, \\ &|G^{(i)} - \langle G \rangle| / \langle G \rangle \ll 1, \\ &|\alpha^{(i)} - \langle \alpha \rangle| / \langle \alpha \rangle \ll 1, \end{aligned} \quad \text{(B-1)}$$

where $\alpha = 1 - K_{\mathrm{Dry}}/K_s$ is the Biot and Willis (1957) coefficient and the superscript i refers to the properties of ith layer. Because their variations are small, the elastic properties of the upscaled

medium can then be approximated by arithmetic averages as $\bar{K}_{\text{Dry}} = \langle K_{\text{Dry}} \rangle$, $\bar{G} = \langle G \rangle$, and $\bar{\alpha} = \langle \alpha \rangle$. As a result, Gassmann's (1951) fluid-substitution equation assuming hydraulic isolation between layers can be written as (Norris, 1993; Wollner and Dvorkin, 2016)

$$\bar{K} = \bar{K}_{\text{Dry}} + \bar{\alpha}^2 \langle M \rangle, \tag{B-2}$$

where

$$M = \left[\frac{\phi}{K_f} + \frac{\alpha - \phi}{K_s} \right]^{-1}. \tag{B-3}$$

Let us now ask ourselves what will $\bar{K}_f$ obtained from equation B-2 be if $\langle M \rangle$ used in this equation is

$$\bar{M} = \left[\frac{\bar{\phi}}{\bar{K}_f} + \frac{\bar{\alpha} - \bar{\phi}}{\bar{K}_s} \right]^{-1}. \tag{B-4}$$

Then, from equations B-2 and B-4, we find

$$\frac{\bar{K}_f}{\bar{\phi} + \frac{\bar{K}_f(\bar{\alpha} - \bar{\phi})}{\bar{K}_s}} = \left\langle \frac{K_f}{\phi + \frac{K_f(\alpha - \phi)}{K_s}} \right\rangle. \tag{B-5}$$

Assume next that

$$\frac{\bar{K}_f(\bar{\alpha} - \bar{\phi})}{\bar{K}_s} \ll \bar{\phi} \tag{B-6}$$

and

$$\frac{K_f(\alpha - \phi)}{K_s} \ll \phi, \tag{B-7}$$

which is plausible in rock with high mineral bulk modulus and medium to high porosity. As a result, equation B-5 becomes

$$\bar{K}_f = \left\langle \frac{K_f}{\phi} \right\rangle \bar{\phi}. \tag{B-8}$$

If we further assume that

$$|\phi^{(i)} - \bar{\phi}| / \bar{\phi} \ll 1, \tag{B-9}$$

this equation becomes

$$\bar{K}_f = \langle K_f \rangle. \tag{B-10}$$

REFERENCES

Angeleri, G. P., and R. Carpi, 1982, Porosity prediction from seismic data: Geophysical Prospecting, **30**, 580–607, doi: 10.1111/j.1365-2478.1982.tb01328.x.

Arévalo-López, H. S., and J. P. Dvorkin, 2016, Porosity, mineralogy, and pore fluid from simultaneous impedance inversion: The Leading Edge, **35**, 423–429, doi: 10.1190/tle35050423.1.

Arévalo-López, H. S., and J. P. Dvorkin, 2017, Simultaneous impedance inversion and interpretation for an offshore turbiditic reservoir: Interpretation, **5**, no. 3, SL9–SL23, doi: 10.1190/INT-2016-0192.1.

Avseth, P., T. Mukerji, and G. Mavko, 2005, Quantitative seismic interpretation: Applying rock physics tools to reduce interpretation risk: Cambridge University Press.

Bachrach, R., 2006, Joint estimation of porosity and saturation using stochastic rock-physics modeling: Geophysics, **71**, no. 5, O53–O63, doi: 10.1190/1.2235991.

Backus, G. F., 1962, Long-wave elastic anisotropy produced by horizontal layering: Journal of Geophysical Research, **67**, 4427–4440, doi: 10.1029/JZ067i011p04427.

Biot, M. A., and D. G. Willis, 1957, The elastic coefficients of the theory of consolidation, Journal of Applied Mechanics, 24, 594–601.

Bortoli, L. J., F. Alabert, A. Haas, and A. Journel, 1992, Constraining stochastic images to seismic data: Stochastic simulation of synthetic seismograms, in A. Soares, ed., Geostatistics troia: Kluwer Academic Publishers, 325–337.

Brie, A., F. Pampuri, A. F. Marsala, and O. Meazza, 1995, Shear sonic interpretation in gas-bearing sands: Presented at the SPE Annual Technical Conference and Exhibition, 701–710.

Buland, A., and H. Omre, 2003, Bayesian linearized AVO inversion: Geophysics, **68**, 185–198, doi: 10.1190/1.1543206.

Cadoret, T., 1993, Effet de la saturation eau/gaz sur les propriétés acoustiques des roches: Ph.D. thesis, University of Paris.

Dolberg, D. M., J. Helgesen, T. H. Hanssen, I. Magnus, G. Saigal, and B. K. Pedersen, 2000, Porosity prediction from seismic inversion, Lavrans Field, Halten Terrace, Norway: The Leading Edge, **19**, 392–399, doi: 10.1190/1.1438618.

Domenico, S. N., 1976, Effect of brine-gas mixture on velocity in an unconsolidated gas reservoir: Geophysics, **41**, 882–894, doi: 10.1190/1.1440670.

Doyen, P., 2007, Seismic reservoir characterization: An Earth modelling perspective: European Association of Geoscientists & Engineers Publications.

Dvorkin, J., M. Gutierrez, and D. Grana, 2014, Seismic reflections of rock properties: Cambridge University Press.

Dvorkin, J., and U. Wollner, 2017, Rock-physics transforms and scale of investigation: Geophysics, **82**, no. 3, MR75–MR88, doi: 10.1190/geo2016-0422.1.

Eidsvik, J., P. Avseth, H. Omre, T. Mukerji, and G. Mavko, 2004, Stochastic reservoir characterization using prestack seismic data: Geophysics, **69**, 978–993, doi: 10.1190/1.1778241.

Gassmann, F., 1951, Über die elastizität poröser medien: Vierteljahrsschrift der Naturforschenden Gesellschaft in Zürich, **96**, 1–23.

Grana, D., 2016, Bayesian linearized rock-physics inversion: Geophysics, **81**, no. 6, D625–D641, doi: 10.1190/geo2016-0161.1.

Grana, D., and E. Della Rossa, 2010, Probabilistic petrophysical-properties estimation integrating statistical rock physics with seismic inversion: Geophysics, **75**, no. 3, O21–O37, doi: 10.1190/1.3386676.

Haas, A., and O. Dubrule, 1994, Geostatistical inversion: A sequential method of stochastic reservoir modeling constrained by seismic data: First Break, **12**, 561–569, doi: 10.3997/1365-2397.1994034.

Han, D. H., 1986, Effects of porosity and clay content on acoustic properties of sandstones and unconsolidated sediments: Ph.D. thesis, Stanford University.

Hill, R., 1952, The elastic behavior of crystalline aggregate: Proceedings of Physical Society, London A, **65**, 349–354, doi: 10.1088/0370-1298/65/5/307.

Marion, D., and D. Jizba, 1997, Acoustic properties of carbonate rocks: Use in quantitative interpretation of sonic and seismic measurements, in I. Palaz, and K. J. Marfurt eds., Carbonate seismology: SEG, 75–93.

Mavko, G., and K. Bandyopadhyay, 2009, Approximate fluid substitution for vertical velocities in weakly anisotropic VTI rocks: Geophysics, **74**, no. 1, D1–D6, doi: 10.1190/1.3026552.

Mukerji, T., A. Jørstad, P. Avseth, G. Mavko, and J. R. Granli, 2001, Mapping lithofacies and pore-fluid probabilities in a North Sea reservoir: Seismic inversions and statistical rock physics: Geophysics, **66**, 988–1001, doi: 10.1190/1.1487078.

Norris, A. N., 1993, Low-frequency dispersion and attenuation in partially saturated rocks: Journal of the Acoustical Society of America, **94**, 359–370.

Russell, B., 1988, Introduction to seismic inversion methods: SEG.

Sams, M. S., and D. Saussus, 2010, Comparison of lithology and net pay uncertainty between deterministic and geostatistical inversion workflows: First Break, **28**, 35–44, doi: 10.3997/1365-2397.2010005.

Sen, M. K., and P. L. Stoffa, 2013, Global optimization methods in geophysical inversion: Cambridge University Press.

Sengupta, M., and R. Bachrach, 2007, Uncertainty in seismic-based pay volume estimation: Analysis using rock physics and Bayesian statistics: The Leading Edge, **26**, 184–189, doi: 10.1190/1.2542449.

Spikes, K., T. Mukerji, J. Dvorkin, and G. Mavko, 2007, Probabilistic seismic inversion based on rock-physics models: Geophysics, **72**, no. 5, R87–R97, doi: 10.1190/1.2760162.

Wollner, U., and J. Dvorkin, 2016, Effective fluid and grain bulk moduli for heterogeneous thinly layered poroelastic media: Geophysics, **81**, no. 6, D573–D584, doi: 10.1190/geo2016-0088.1.

Wollner, U., Y. Yang, and J. P. Dvorkin, 2017, Rock physics diagnostics of an offshore gas field: Geophysics, **82**, no. 4, MR121–MR132, doi: 10.1190/geo2016-0390.1.